Adsorption in Single-Walled Carbon Nanotubes by Experiments and Molecular Simulation II: Effect of Morphology and Temperature on Organic Adsorption

Sandeep Agnihotri,[1] Massoud Rostam-Abadi,[2,4] Jose' P. B. Mota,[3] Mark. J. Rood[4]

[1]Department of Civil and Environmental Engineering, University of Tennessee, Knoxville. sagnihot@utk.edu; [2]Illinois State Geological Survey, 615 E Peabody Dr., Champaign ILmassoud@isgs.uiuc.edu; [3]Requimte/CQFB, Departamento de Quimica, Faculdade de Ciencias e Tecnologia, Univerdade Nova de Lisboa, 2829-516, Caparica, Portugal pmota@dq.fct.unl.pt; [4]Department of Civil and Environmental Engineering, University of Illinois, Urbana mrood@uiuc.edu

Abstract

In this study, hexane adsorption on single-walled carbon nanotube (SWNT) bundles was studied using the methodology developed in part I of this series of papers. First, hexane adsorption capacities of two purified SWNT samples was gravimetrically determined at isothermal conditions of 25, 37 and 50 ^{o}C for 10^{-4} < p/p_o < 0.9, where p/p_o is hexane vapor pressure relative to its saturation pressure. Next, simulation of hexane adsorption under similar temperature and pressure conditions were performed on the external and internal sites of nanotube bundles of diameters same as those in experimental samples. The internal adsorption was adjusted to incorporate the information about the fraction of open nanotubes present in the sample, as determined in part I; and total adsorption was calculated by summation of external and internal adsorption in the bundles. Comparison of experimental and simulated hexane adsorption capacities demonstrated the soundness of the methodology developed in part I, importance of organic adsorption on the peripheral surface of the bundles, limiting adsorption capacities of samples and effect of temperature on organic adsorption in nanotubes.

1. Introduction

In this study, adsorption mechanisms and capacities of organic molecules on SWNTs are investigated by experiments and molecular simulation. Grand canonical Monte Carlo (GCMC) simulation of hexane adsorption on SWNTs was carried out and the results are compared to an experimental study[1]. The simulation procedure was developed as part of our previous research on structural characterization of SWNT bundles,[2] where calculations could accurately predict experimental N_2 adsorption isotherms (77 K) of two nanotube samples. Here we demonstrate that the same methodology can be applied to calculate organic adsorption isotherms of SWNT samples, such that a near perfect replication of experimental isotherms is obtained at various isothermal conditions. This establishes the soundness and versatility of simulation procedure developed earlier.[2] Hexane adsorption on external surface of SWNT bundles, inside nanotubes and the effect of temperature on adsorption is studied. It is found that the experimentally observed lowering of hexane capacity of SWNT samples at higher temperatures is primarily due to decreased adsorption on the external surface of the bundles and not inside the nanotubes. We could also calculate the limiting hexane adsorption capacities of our samples and predict isotherms for a hypothetical scenario where all nanotubes in a sample would be open. Additionally, it was found that simulated hexane isotherms complemented experimental isotherms of other organic compounds also,[2] which

showed that hexane adsorption mechanisms explored in this study could very likely be the general adsorption mechanisms for most organic vapors on SWNTs.

2. Experiments, Simulation and Analytical Methods

GCMC simulations were performed to predict hexane adsorption on two commercially available purified samples of SWNTs. Sample description and characterization details are available elsewhere.[3] Brief description of those results is presented here for clarity. SWNT samples selected for this study were synthesized by two methods: electric-arc and HiPco chemical vapor deposition (CVD).[4,5] Both samples were produced by the manufacturer from purification of as-grown nanotubes. The electric-arc sample contained 95-98 wt% SWNTs (EA95), and the HiPco CVD sample contained ≈ 80 wt% nanotubes (CVD80). The diameter distribution of SWNTs in both samples was determined by Raman analysis. It was found that majority of SWNTs in sample EA95 were 15.2 Å in diameter and those in sample CVD80 were 9 Å wide (Table 1).

Table 1. Morphology of SWNT samples.

| Sample | Wt%[1] | | Diameter (Å)[2] | Relative amount[2] |
	SWNTs	Impurities		
EA95	95 - 98	3 - 5	11.5	1.0
			14.0	2.3
			15.2	3.5
CVD80	~80	~20	9.0	4.3
			10.2	2.2
			10.7	1.7
			11.1	1.1
			11.8	1.0

[1] Manufacturer specified information; [2] Determined from Raman spectroscopy

(a)

(b)

Figure 1. Cross section of unit simulation box for GCMC study of nitrogen adsorption onto different adsorption sites of a bundle of open-ended SWNTs: (a) external groove sites and external surfaces, (b) the internal (endohedral) and interstitial channels. The shaded area represents the effective volume probed during the simulation.
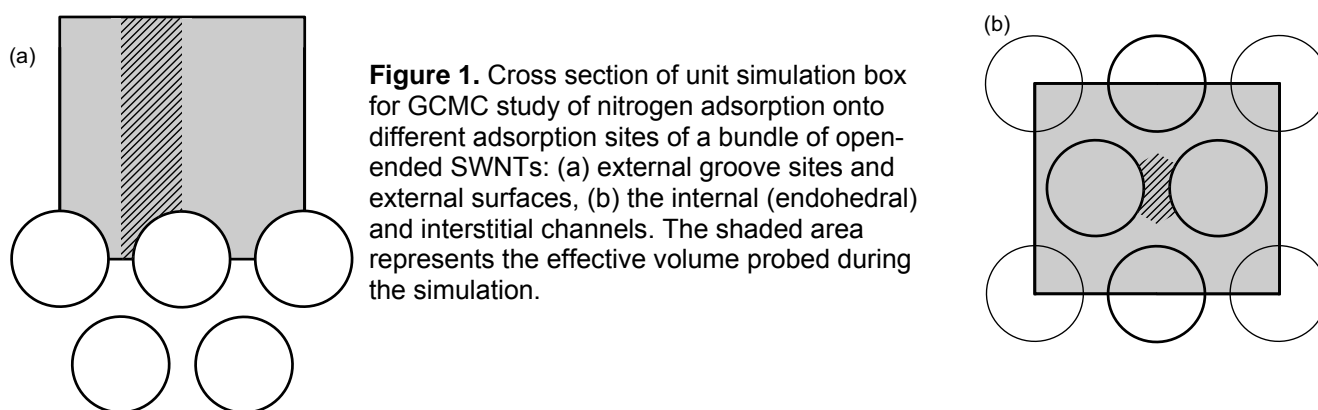
Hexane adsorption isotherms on samples EA95 and CVD80 were determined gravimetrically in an earlier study, the details of which can be found elsewhere.[1] The isotherms were obtained at 298.15 K, 310.15 K and 323.15 K and at vapor concentrations ranging from 1 x 10^{-4} to 0.9 P/P_o, where P is the actual vapor pressure and P_o is the saturation vapor pressure at a particular temperature. The adsorption isotherms are presented later in this manuscript. Simulations were carried out to model experimental conditions. The simulation procedure was

developed previously to predict experimental N_2 adsorption isotherms (77 K) on samples EA95 and CVD80. A detailed discussion of the method can be found elsewhere[1] and following is a brief description of adsorbent model and the analytical approach. Simulations were performed on homogenous arrays of SWNTs of diameters same as those in experimental samples (Table 1). Total adsorption on a bundle was calculated in two steps; external adsorption: adsorption on the external surface of the nanotube bundles (i.e., grooves and peripheral surface, Figure 1a), and internal adsorption: adsorption inside the bundles (i.e., intratube and in the interstitial channels, Figure 1b). The intertube distance for all simulations was kept fixed at 3.4 Å to imitate SWNTs adhering to each other by van der Waals interaction.

Once the external and internal adsorption capacities of homogenous bundles were determined by simulation, the total adsorption, $q_{sim}(P/P_o)$, for a sample was calculated by averaging the adsorption contribution from bundles of nanotube sizes relevant to that sample:

$$q_{sim}(P/P_o) = S_P \, q_{sim}^s(P/P_o) + \alpha(1-\eta)q_{sim}^i(P/P_o) \tag{1}$$

$$\{q_{sim}^s, q_{sim}^i\} = \sum_{D=sample} w_D \{q_{sim,D}^s, q_{sim,D}^i\}(P/P_o) \tag{2}$$

where, S_P is the external surface area of nanotube bundles in the sample (m²/g), and $q_{sim,D}^s(P/P_o)$ and $q_{sim,D}^i(P/P_o)$ are adsorption capacities for the external surface (s) and internal volume (i) of a homogeneous bundle of nanotube diameter, D at a relative vapor pressure P/P_o, 100η is the wt% of impurities in the sample, w_D is the weight fraction of nanotubes of diameter, D (Table 1), and α is a scaling parameter that adjusts an entire internal adsorption isotherm to yield a total isotherm which fits the experimental isotherm. This parameter is termed as the fraction of open-ended nanotubes in the sample. It should be noted that $q_{sim}(P/P_o)$ and $q_{sim,D}^i(P/P_o)$ are calculated as amount adsorbed per unit mass of nanotubes, however, $q_{sim,D}^s(P/P_o)$ is estimated as amount adsorbed per unit external surface area of the bundle. $q_{sim,D}^s(P/P_o)$ was found to be insensitive to D, which was an important result as it would obviate the need to simulate external adsorption on nanotube bundles of every value of D, as long as adsorption is governed by Lennard-Jones interactions. S_P and α are structural parameters of a sample. S_P was obtained as the slope of $q_{sim,D}^s(P/P_o)$ versus $q_{exp}(P/P_o)$ plot, where $q_{exp}(P/P_o)$ is the experimental isotherm of the sample. α was calculated as the ratio of experimental micropore volume to $(1-\eta)q_{sim}^i(P/P_o)$. Notice that $q_{sim,D}^i(P/P_o)$ would be the maximum theoretical micropore volume of a sample, after removing all impurities and opening all nanotubes. S_P and α for samples EA95 and CVD80 are provided in Table 2, and are used here for calculation of hexane adsorption on same samples.

Table 2. Structural parameters for SWNT samples.

Sample	S_P (m²/g)	α
EA95	160	0.45
CVD80	437	0.60

In this research, $q^s_{sim,D}(P/P_o)$ and $q^i_{sim,D}(P/P_o)$ are calculated for adsorption of hexane molecules on nanotube arrays. Hexane molecule is modeled as a flexible chain of pseudo-atoms. The molecular force field adopted for interaction sites of hexane is the transferable potential for phase equilibria (TraPPE) force field.[6-8] This force field is based on a united-atom description where carbon and its bonded hydrogens are combined into a single interaction site, leading to introduction of CH_4, CH_3, CH_2, CH and C pseudoatoms. The non-bonded interactions between such pseudoatoms are described by the Lennard-Jones 12-6 potential (Eq.3), as is the interaction between carbon atoms of a nanotube.

$$u_{ij}(r) = 4\varepsilon_{ij}\left[(\sigma_{ij}/r)^{12} - (\sigma_{ij}/r)^6\right]$$ (3)

where, r is the intermolecular distance. The well depths ε_i/k_B, where k_B is Boltzmann constant, and collision diameters σ_i used are given in Table 3. Unlike interactions (such as CH_3-**CH_2**-CH_2) are computed from the standard Lorenz-Berthelot combining rules: $\varepsilon_{ij} = \sqrt{\varepsilon_i\varepsilon_j}$ and $\sigma_{ij} = (\sigma_i + \sigma_j)/2$.

Table 3. Lennard-Jones potential parameters.

Site–site	ε/k_B (K)	σ (Å)
C-C	28	3.40
CH_3-CH_3	98	3.75
CH_3-CH_2	98	3.75
CH_2-CH_2	46	3.95

Adjacent pseudoatoms are connected by a fixed C-C bond length of 1.54 Å with a bond angle bending governed by a harmonic potential,

$$U_{Bend} = k_\theta(\theta - \theta_o)^2/2$$ (4)

where U_{Bend} is the bond angle bending potential, force constant k_θ/k_B = 62,500 K rad^{-2} and the equilibrium bond angle, θ_o = 114°. The motion of the dihedral angles, ϕ, is governed by the optimized potentials for liquid simulations (OPLS) torsion potentials for united atoms,

$$U_{tors} = \frac{c_1}{2}[1 + \cos\phi] + \frac{c_2}{2}[1 - \cos(2\phi)] + \frac{c_3}{2}[1 + \cos(3\phi)]$$ (5)

where U_{tors} is the torsion potential and c_1/k_B = 710.06 K, c_2/k_B = -136.38 K and c_3/k_B = 1582.64. To enhance the sampling of configurational space and increase the acceptance rate of the particle insertion/removal step, we resort to configurational-bias sampling techniques (Frenkel and Smit, 1996). The configurational-bias GCMC method produces chain configurations one pseudo-atom at a time through a two step process. The first step is to generate a number of candidate positions for the bead on the surface of a sphere. Candidate positions are selected from random variates according to the energy contributions from internal

degrees of freedom (i.e. bond and dihedral angles). The second step is to select one of these candidates according to the energy contributions from the remaining external degrees of freedom. There are three cases of fragment addition that occur during a hexane molecule construction; they all involve the placement of single pseudo-atom fragments. The first case, which is termed *first atom sampling*, occurs when the first CH_3 pseudo-atom of the molecule is being placed. The second case, called sphere sampling, occurs only for the second pseudo-atom of the molecule, which is a CH_2 bead. The third case, known as *disk sampling*, occurs for the straight chain portion of the hexane molecule, when the placement of a bead involves a single bond angle (Figure 2).

Figure 2. Schematic of disk sampling technique for placement of pseudoatom *j*.
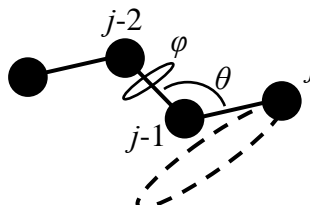
The placement of the first CH_3 pseudo-atom follows the same rules employed for placing a single nitrogen molecule. Sphere sampling is used to place the CH_2 pseudo-atom of the hexane molecule at a fixed bond length $l = 1.54$ Å from the initial CH_3 pseudo-atom. All possible locations of the CH_2 bead must be on the surface of a sphere of radius l centered at the position of the first bead. Disk sampling is used for the placement of the remaining CH_2 pseudo-atoms and the terminal CH_3 pseudo-atom, and must take into account hard and soft energy contributions. Examples of hard contributors include bond lengths and bond angles. Other energy contributors, such as dihedral angles and non-bonded interactions, are weaker functions of position and thus are designated as soft energy contributors. Since bond lengths are fixed in the TraPPE model, bond angles are the only hard contributors. Thus, the placement of a CH_2 pseudo-atom involves the selection of one hard energy contributor (bond angle θ) and one soft contributor (dihedral angle φ). The hard degree of freedom (θ) is always selected first. Having selected a bond angle, the dihedral angle φ is selected by choosing several random positions on the edge of the disk which forms the base of a cone with apex at r and slant height equal to the bond length l. Besides the usual trial step of molecule insertion/deletion, whose acceptance rate is enhanced by resorting to configurational-bias techniques, three additional types of Monte Carlo (MC) moves involving only individual molecules are necessary to sample the internal configuration of the simulation box: translation, rotation about the center-of-mass, and configurational-bias regrowth to change the internal conformation of the molecule.[9] Simulations were carried out at 298.15 K, 310.15 K and 323.15 K for $10^{-8} \leq P/P_o \leq 0.9$. Each run was equilibrated for 2×10^4 MC cycles followed by 3×10^4 MC cycles for the production period. The maximum displacement for translation in the simulation box was adjusted during the equilibration phase to give a 50% acceptance rate. Standard deviations of the ensemble averages were computed by breaking the production run into five blocks.

3. Results and Discussion

3.1. External Adsorption

Hexane adsorption on the external surface of SWNT bundles ($q^s_{sim,D}(P/P_o)$) was determined for bundles of D = 9 Å. This diameter was chosen arbitrarily as external adsorption

was earlier found to be independent of nanotube size.[2] The simulation data was considered sufficient to represent all nanotube sizes (Table 1) and both SWNT samples. It should be noted that the absolute external adsorption (i.e., the amount adsorbed outside the bundles per unit mass of nanotubes, $S_P\, q^s_{sim}(P/P_o)$ in Eq.1,) would still be different for both samples, due to different values of S_P (Table 2). The isotherms were calculated at 298.15 K, 310.15 K and 323.15 K, and are presented in Figure 3. It was observed that hexane does not adsorb on the peripheral surface of the bundles until $P/P_o \approx 5 \times 10^{-5}$, and perceptible external adsorption ($\geq$ 10% of adsorption at $P/P_o \approx 0.9$) is obtained only when P/P_o was raised to 10^{-2}. This result validates the hypothesis made in the experimental study of organic adsorption on samples EA95 and CVD80,[1] where it was suggested that the total adsorption capacity of a sample at low vapor pressures would mainly be dominated by adsorption in the pores of nanotubes and not on their external surface. The effect of temperature was evident from decrease in external adsorption when the temperature was raised from 298.15 K to 323.15 K. This is typical for exothermic physical adsorption. However, it also noticed that the difference in external adsorption capacity due to temperature increase was more pronounced at lower vapor pressures, and as the gas-phase concentration steadily increased the difference became less noticeable (76% decrease at $P/P_o \approx 1 \times 10^{-4}$ as opposed to 20% decrease at $P/P_o \approx 0.9$). This is because as the vapor concentration increases, multi-layer adsorption starts to occur and nanotubes begin to lose their effect on adsorbate molecules farthest from the bundle surface.

Figure 3. Effect of temperature on hexane adsorption on the peripheral surface of a homogeneous nanotube bundle comprising 9 Å SWNTs.
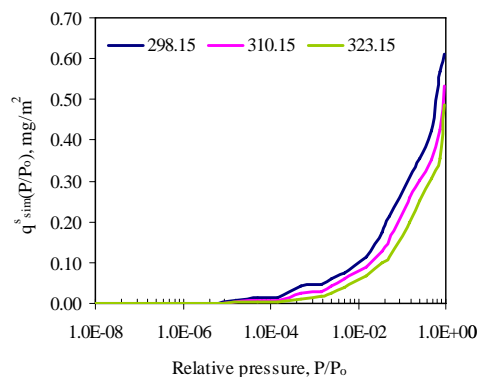
3.2. Internal Adsorption

Hexane adsorption inside a homogeneous array of nanotubes ($q^i_{sim,D}(p/p_o)$) was calculated for homogeneous bundles of all SWNT diameters (Table 1). The resulting adsorption isotherms are presented in Figure 4. It was observed that for $P/P_o \geq 10^{-6}$, wide nanotubes would have higher adsorption capacity than thin nanotubes. This is to say that samples with large diameter SWNTs will be more suitable adsorbents when target organic vapor is present in concentrations in excess of 100's of ppbv. Second, adsorption in all bundles continued to steadily increase with increasing vapor concentration even when the gas-phase concentration was close to saturation. This behavior is different from adsorption of N_2 in nanotubes where bundles were completely saturated at P/P_o well below saturation ($P/P_o = 10^{-6}$ for D = 9 Å and $P/P_o = 10^{-3}$ for D = 15.2 Å).[2] It is believed that this difference in adsorption trends arises due to the fact that a hexane molecule is much bigger than a N_2 molecule, which gives the former the advantage to reorient and, therefore, continue to pack with increasing concentration.
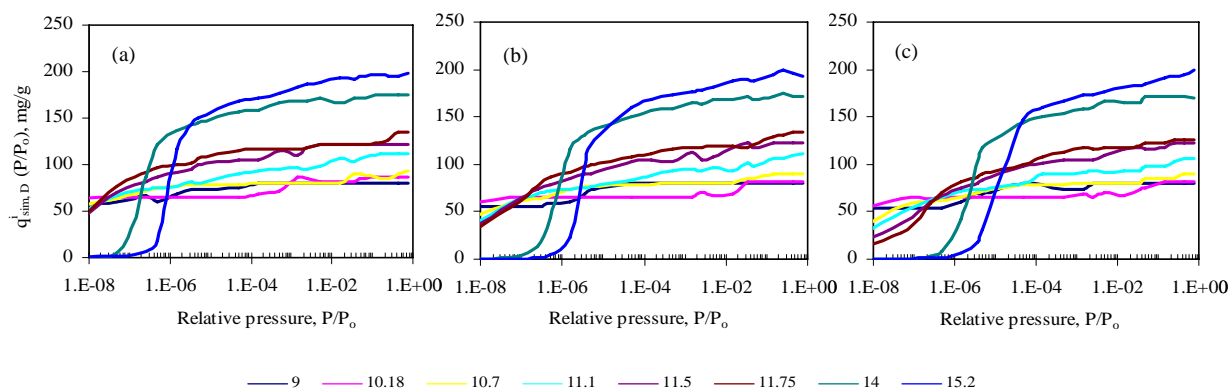
Figure 4. Internal adsorption isotherms of hexane in homogeneous bundles of SWNTs of diameter relevant to samples EA95 and CVD80 at (a) 298.15 K (b) 310.15 K and (c) 323.15 K. The lower horizontal legend describes the SWNT diameters in Å.

The effect of temperature on internal adsorption capacity of bundles was peculiar (Figure 4). It appeared that increasing temperature caused only a slight decrease in adsorption capacities for $P/P_o \leq 10^{-6}$, above which adsorption in a bundle remained almost unaffected with temperature. This trend seems unique to nanotubes which, to the best of our knowledge, has not been reported for activated carbons. It is believed to be due to a regular matrix-like structure of cylindrical pores in SWNT bundles, which have a deeper well depth (i.e., stronger interaction with hexane molecules) than slit shaped pores in activated carbons. Although, it is advised that these results might be true for the temperature range tested in this study, which was well below the boiling point of hexane (341.9 K).

3.3 Total Adsorption

The total hexane adsorption capacities of each sample were calculated by summing their external and internal adsorption contributions according to Eq.1. The external surface areas of bundles (S^p) and scaling parameter for internal adsorption (α) were taken to be the same as those obtained previously from N_2 adsorption simulations (Table 2). The isotherms were calculated for samples EA95 and CVD80 at 298.15 K, 310.15 K and 323.15 K, and are presented in Figure 5 along with the experimental isotherms measured in a previous study.[1] It was noticed that the simulated isotherms replicated the experimental isotherms for both samples and at all tested temperatures (Figure 5). Such agreement demonstrates the versatility of the simulation procedure and the analytical techniques developed in our previous study.[2] Numerous observations can be made by comparing theoretical and experimental isotherms. First, internal adsorption dominates the total adsorption capacity of sample EA95 while external adsorption is more significant for sample CVD80; and external adsorption on sample CVD80 becomes noticeable at lower P/P_o. This trend is a direct effect of differences in morphologies of nanotubes in two samples. Large diameter nanotubes (sample EA95) have more internal pore volume and less external surface area whereas narrow nanotubes (sample CVD80) have less internal pore volumes but large bundle area (Table 1). Second, at very low vapor concentrations ($10^{-8} < P/P_o < 10^{-6}$ or 2 to 200 ppb) sample CVD80 would have much higher organic vapor adsorption capacities than sample EA95 as narrow nanotubes could be filled at lower vapor concentrations (Figure 4). This is an important result which could not be obtained experimentally;[1] and now it can be said that the true potential of nanotubes as

adsorbents for vapors present in extremely low concentrations can be found in samples containing small sized nanotubes. For bulk separation and gas storage, however, large nanotubes will be desirable. Third, the effect of temperature on total adsorption capacity was apparent. In experiments, it was observed that adsorption on samples decreased with temperature, however, exact reason for which could not be discovered. Simulations showed that this decrease in adsorption capacity is due to an appreciable lowering of adsorption on the peripheral surface of nanotube bundles in samples EA95 and CVD80, and only a marginal decrease in adsorption inside nanotubes (Figure 5). The effect of temperature on total adsorption capacity was more evident for sample CVD80 because external adsorption contributed more in this sample. Therefore, it is reasonable to say that as temperature is raised, adsorption internal sites are preferred (Figure 1). This result also supports the hypothesis made previously[1] that heterogeneous nature of adsorption in nanotubes reduces with temperature.

Figure 5. Simulated hexane adsorption isotherms for samples EA95 (a-c), and CVD80 (d-f) at various isothermal conditions. Notice the near replication of experimental results (circles). R^2 for all figures > 0.95.

Legend: $q_{sim}(P/P_o)$; $q_{exp}(P/P_o)$; $\alpha(1-\eta)q_{sim}^i(P/P_o)$; $S_P\,q_{sim}^s(P/P_o)$
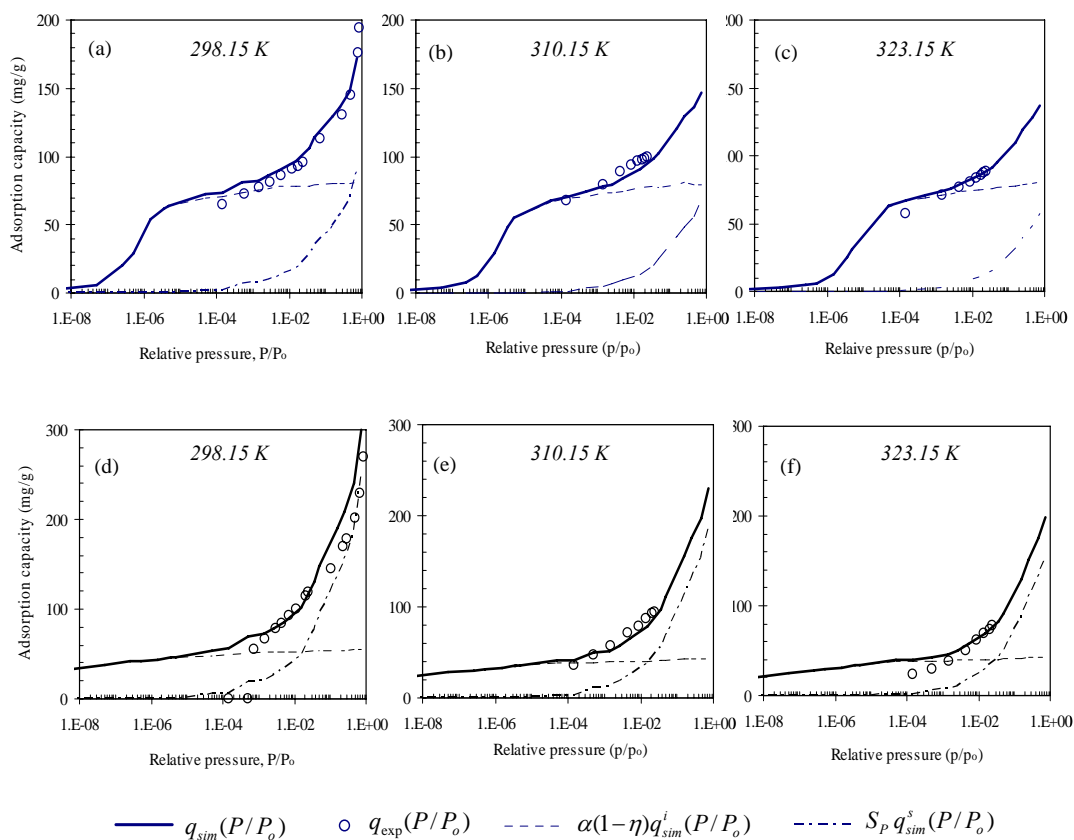
3.4 Limiting Adsorption Capacity

The total hexane adsorption capacities of samples EA95 and CVD80 were extrapolated to a condition where all nanotubes in a sample would be open. This was done by assuming $\alpha = 1$ and recalculating the total isotherm at 298.15 K. The simulated isotherms were presented in Figure 6. It was observed that opening all nanotubes will cause at least a two fold increase in adsorption in sample EA95 and only a marginal increase in adsorption on sample CVD80. Additionally, sample EA95 will have high adsorption capacity for the most P/P_o values except at very low ($P/P_o \le 10^{-6}$) and very high vapor concentration ($P/P_o > 0.1$) when adsorption in

sample CVD80 is more than that in sample EA95. Such as scenario is only hypothetical because, to our understanding, analytical techniques to extract only open-ended nanotubes from as-grown materials still remain to be developed.

Figure 6. Limiting hexane adsorption on samples EA95 (a) and CVD80 (b) at 298.15 K. Total simulated capacities (solid lines) are much higher than experimental values (circles) for both samples, as internal adsorption has not been scaled for the fraction of open-ended nanotubes present in each sample.

$$\text{———}\ q_{sim}(P/P_o) \qquad \circ\ q_{exp}(P/P_o) \qquad \text{- - - -}\ \alpha(1-\eta)q_{sim}^i(P/P_o) \qquad \text{-·-·-}\ S_P\, q_{sim}^s(P/P_o)$$
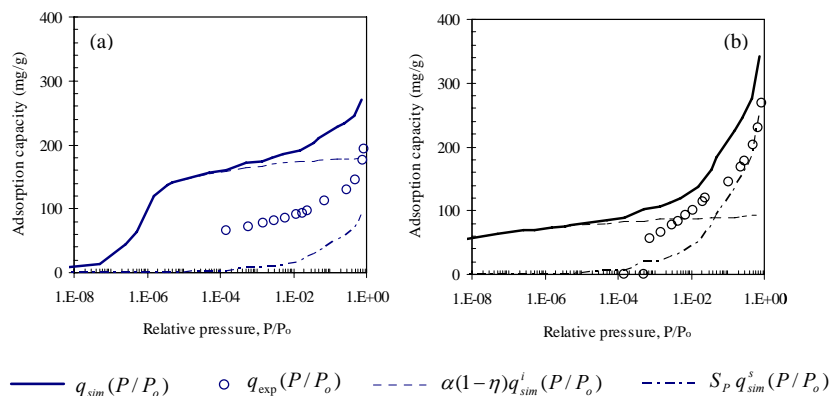
4. Summary and Conclusions

In this study, adsorption of hexane on SWNT bundles was carried out by Monte Carlo simulation. The simulation procedure and analytical methods were developed previously to predict N_2 adsorption (77 K) isotherms of purified SWNT samples.[2] Here we demonstrated that the same methodology could also be applied to calculate hexane adsorption on the external surface of SWNT bundles, inside nanotube bundles, and the total isotherms. A near perfect replication of experimental isotherms was achieved for various samples and at different experimental conditions. The effect of temperature on adsorption was also studied, and it was found that adsorption inside nanotubes is affected only at very low vapor concentrations ($P/P_o \leq 10^{-6}$) and the experimentally observed lowering of hexane capacity of SWNT samples at higher temperatures is due mainly to decreased adsorption on the external surface of the bundles and not inside the nanotubes. The simulations could also predict isotherms for a hypothetical scenario where all nanotubes in a sample would be open. Finally, it was found that simulated hexane isotherms complemented experimental isotherms of other more complex organic compounds, which showed that hexane adsorption mechanisms explored in this study could very likely be general adsorption mechanisms on nanotubes for most organic vapors.

References

1. Agnihotri S, Rood MJ, Rostam-Abadi M. Carbon 2005. 43:2379-2388.
2. Agnihotri S, Mota PB, Rostam-Abadi M, Rood M.J. Langmuir 2005, 21(3):896-904.
3. Agnihotri S, Rostam-Abadi M, Rood MJ. Carbon 2004, 42 (12-13):2699-2710.
4. Nikolaev P, Bronikowski MJ, Bradley RK, Rohmund F, Colbert DT, et al. Chem Phys Lett 1999; 313(1):91-97.
5. Bronikowski MJ, Willis PA, Colbert DT, Smalley RE. J Vac Sci Technol, A 2001; 19(4):1800-1805.
6. Martin GM, Siepmann JI. J. Phys. Chem. B 1998. 102:2569-2577.
7. Martin GM, Siepmann JI. J. Phys. Chem. B 1999. 103:4508-4517.
8. Chen B, Siepmann JI. J. Phys. Chem. B 1999. 103:5370-5379.
9. Frenkel, D.; Smit, B. Understanding Molecular Simulation (Academic Press, London, 1996).